Four Channels in the Fission of ^{252}Cf

U. Brosa, S. Grossmann, and A. Müller
Fachbereich Physik der Philipps-Universität, Marburg, West Germany

Z. Naturforsch. **41 a**, 1341 – 1346 (1986); received September 25, 1986

Strutinsky-type calculations indicate that the potential energy favors four channels in the nuclear fission of ^{252}Cf. The connection of this finding with experimental results on the distribution of fragment mass, total kinetic energy, neutron multiplicities, and relative abundances is discussed. Similar calculations for ^{227}Ac, ^{236}U, and ^{258}Fm show that the changing preponderance of the four channels seems to describe striking trends in the fission of the actinides, in particular the dip in the total kinetic energy at symmetrical fission of ^{236}U and the enormously high average kinetic energy of the ^{258}Fm fragments.

1. Introduction

The mass yield curve of the fission of ^{232}Th induced Turkevich and Niday to postulate the existence of *two fission modes* or *channels* [1]. Britt and coworkers used this suggestion to interpret data on the fission of ^{226}Ra [2]. The underlying idea was that the nucleus might reach two different scission shapes: a short, asymmetrical and a long, symmetrical one. The superposition of fragment yields from these two channels would simultaneously explain mass and kinetic energy distributions. Recently the same idea was applied by Itkis et al. [3] to the fission of the preactinides and by Hulet and coworkers [4] to the very heavy actinides.

We attempt a unified explanation of fission for all nuclei ranging from the preactinides up to the heaviest elements known and suggest, therefore, the existence of not less than *four* fission channels: a very short symmetrical path, two asymmetrical paths of medium length, and a very long symmetrical path. Such channels seem to be present in all actinides. Their accessibility, however, is different for the different nuclei. We present here the channels of ^{252}Cf in detail because ^{252}Cf shows all four channels with greatest distinctness. Some results for ^{236}U and ^{258}Fm will be mentioned to indicate the consistency of our method. The fission channels of ^{227}Ac were also determined, but since they are topologically equal to those of ^{236}U, we will not discuss them here. Part of our work on ^{258}Fm is being published [5].

Reprint requests to Prof. Dr. S. Großmann, Fachbereich Physik der Universität Marburg, D-3550 Marburg, F.R.G.

2. The Computational Method

We computed binding energies by the Strutinsky method for deformed nuclei [6]. Their shapes were parametrized in cylindrical coordinates (r, z) as [7]

$$r^2 = (l_h^2 - z^2)\,(a_0 + a_1 (z - z_n)/r_{cn} + a_2 (z - z_n)^2/r_{cn}^2)\,, \tag{1}$$

where the coefficients a_0, a_1, and a_2 are given by

$$a_0 = r_n^2/(l_h^2 - z_n^2)\,,$$

$$a_1 = 2\,a_0 r_n r_{cn}/(l_h^2 - z_n^2)\,,$$

$$a_2 = (r_{cn}^5 - a_0 l_h^2 r_{cn}^3 + a_1 l_h^2 z_n r_{cn}^2)/(l_h^3 z_n^2 + l_h^5/5)\,. \tag{2}$$

The radius r_{cn} of the compound nucleus may be regarded as fixed, whereas l_h (half of the total length), z_n (location of the neck), and r_n (radius of the neck) define the variability of the shape (see also Figure 2). The shell corrections were done in the standard fashion (cf. [8] for more recent work) using Saxon-Woods single-particle potentials with the parameters recommended by Sobiczewski et al. [9]. The liquid drop part of the binding energy was calculated with the parameters proposed by Myers and Swiatecki [10].

A serious obstacle was Wilets' objection [11]. He pointed out that the interpretation of contour plots of the potential energy may be misleading since the only features which remain unchanged under a coordinate transform are stationary points. The criticism is all the more urgent if we have more than two degrees of freedom. If we wish to produce a contour plot, we have to choose by more or less

0340-4811 / 86 / 1200-1341 $ 01.30/0. – Please order a reprint rather than making your own copy.

arbitrary criteria a two-dimensional manifold in the coordinate space. To overcome these difficulties, we minimized the negative binding energy as a function of l_h, z_n, and r_n with the constraint

$$q_l \cdot (l_h - l_{ho}) + q_r \cdot (r_n - r_{no}) + q_z \cdot (z_n - z_{no}) = 0\,, \quad (3)$$

where (q_l, q_r, q_z) may be construed as a vector which is perpendicular to the plane of minimization. Usually we had $(q_l, q_r, q_z) = (1, 0, 0)$, i. e. l_h was fixed, and r_n and z_n were adapted. Shifting (l_{ho}, r_{no}, z_{no}) through the (l_h, r_n, z_n)-space and minimizing over and over again yielded points in that space. When these points were close enough, they were connected and a preliminary picture of the channels was obtained. Furthermore for some points on every channel we took the respective tangent from the preliminary picture, constructed about this tangent a cone with an apex of 90°, chose the vector (q_l, q_r, q_z) from the interior of this cone, and repeated minimization. A channel was accepted only if its points remained the same within limits of $\pm$ 0.5 fm.

Other checks examining the variability of the shape parametrization, the parameters of the single-particle potentials, and the efficiency of the smearing procedure will be described elsewhere.

3. Results and Comparison with Experiments

Our results are displayed in Figure 1. Since the channels pass through the three-dimensional space (l_h, r_n, z_n), three projections on the (l_h, r_n), (r_n, z_n), and (l_h, z_n) planes are shown. The potential energy of the deformed nucleus, defined as excess of the ground-state binding energy E_{gs} over the binding energy E_{def} of the deformed nucleus, is given as a function of l_h. There are four channels in these projections. The channel marked by the solid lines is the "standard path". It connects the ground state (gs) with a decaying shape (+) via the lowest barrier. The "super-long path" is discriminated by dashed lines. It branches off from the standard path shortly before the latter enters the "great loop", where the nucleus would shorten while it diminishes its radius r_n. For $l_h > 25$ fm no minima can be found. The super-long path, however, already terminates at $l_h = 20.7$ fm since we find at this point an absolute minimum of the potential energy (cf. Fig. 1), and the barrier which saves the nucleus from strangulation is there quite low ($\lesssim$ 2 MeV, cf. Figure 4). The "super-short path" is indicated by the dotted lines. It bifurcates from the standard path when the shortening is most effective and ends at $l_h = 14$ fm. Figure 2 visualizes typical shapes which belong to these paths. The dash-dotted lines, finally, represent the "super-asymmetrical path". It starts directly from the ground state and finishes at $l_h = 15.7$ fm. The respective shapes look like compromises between those of the standard and super-long paths, however with much larger asymmetry.

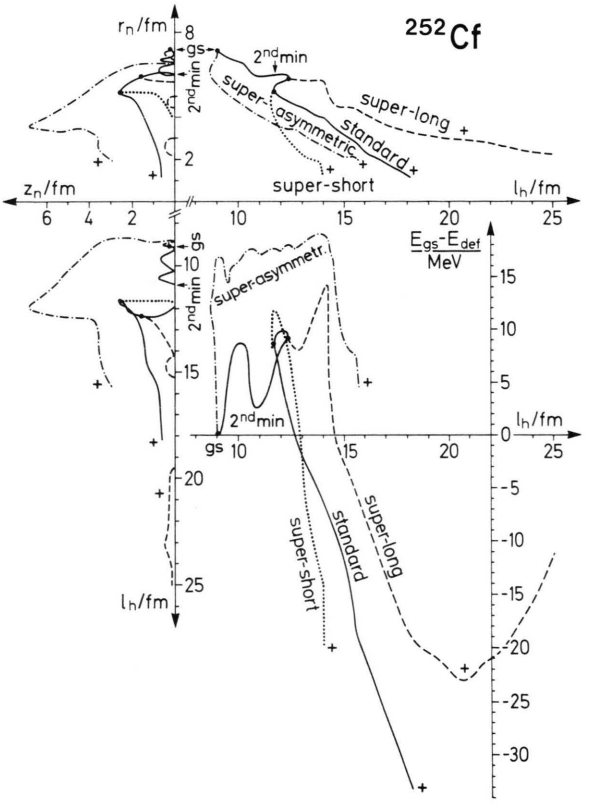

Fig. 1. Survey on the channels in the fission of ^{252}Cf. The top right part shows their projection onto the (r_n, l_h) plane, the top left-hand side gives the view on the (z_n, r_n) plane, and the bottom left-hand side on the (l_h, z_n) plane. The bottom right picture displays the potential energy $E_{gs} - E_{def}$ of the deformed nucleus in excess over the ground-state binding energy E_{gs}. Peculiar points on the channels are distinguished by symbols (gs for ground state, 2^{nd} min for second minimum, heavy dots for branching points, and + for the termination of a channel). The numerical accuracy should be better than 0.5 fm, except for the piece of the super-long channel with $l_h > 21$ fm. This piece is anyhow unphysical.

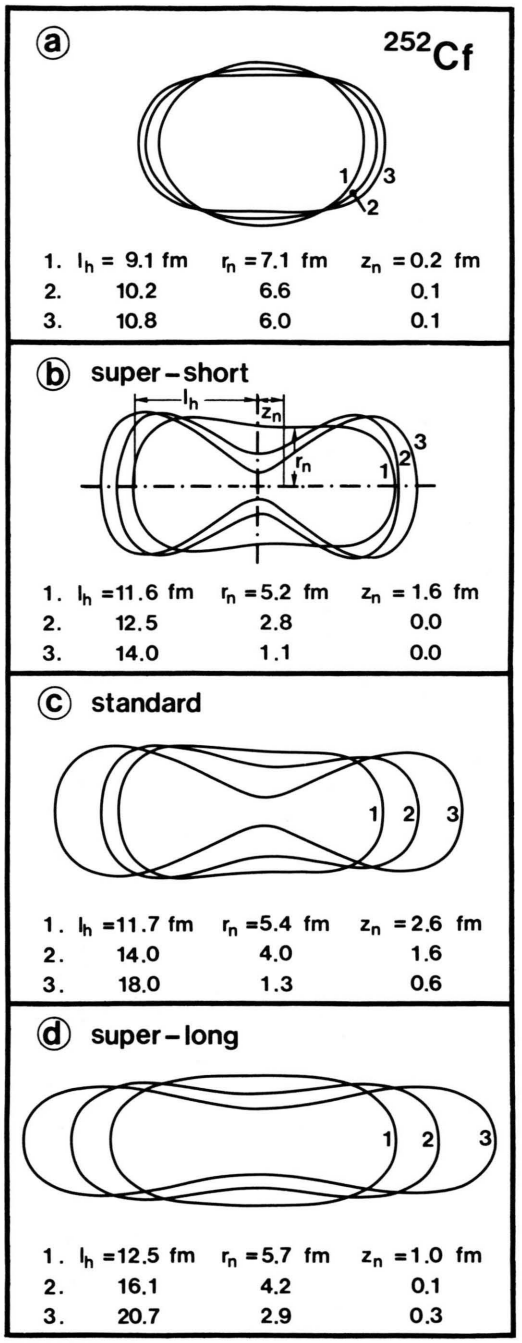

Fig. 2. Visualization of the channels of Figure 1. Part **a** displays the evolution from the ground state (shape 1) to the second minimum (shape 3). Shape 1 of part **b** corresponds to the bifurcation of the super-short path from the standard path, shape 3 then indicates the end of the super-short path. Part **c** describes the standard path with shape 1 being the most asymmetrical shape in this channel, finally part **d** shows the evolution of the super-long channel starting with the branching from the standard path.

Figure 1 allows qualitative and quantitative predictions on several observables: asymmetry of the mass distribution, total kinetic energies, neutron multiplicities, and the relative abundances of the four components.

a) Mass Asymmetry

From the (r_n, z_n) and the (l_h, z_n) planes in Fig. 1 it is seen that only the standard and the super-asymmetrical paths retain asymmetry until scission. Recent experimental results reproduced in Fig. 3 show also two asymmetrical components [12, 13]. To facilitate quantitative comparison between theory and experience, several points from the standard and the super-asymmetrical paths were taken, and the respective values of the neck position z_n were transformed to mass numbers A of the "lighter fragment" defined by the requirement that all mass located between $z = z_n$ and $z = l_h$ should belong to that "fragment". The results are given in Table 1 together with the experimental values $\bar{A}_L$. The largest attainable asymmetries at $l_h = 11.5$ fm and $l_h = 11$ fm are obviously much too large, the asymmetries at scission ($l_h = 18.3$ fm and $l_h = 15.7$ fm) slightly smaller than the experimental results. It would be sufficient if a small part of the too large asymmetry would survive, due to inertia, until scission.

Similar calculations for ^{236}U and ^{258}Fm suggest the following conclusions: There seems to be no asymmetry along the most probable path for ^{258}Fm,

Table 1. Mass number A of the light "fragment" in the standard and the super-asymmetric channels. The experimental values $\bar{A}_L$ are entered just below the computed mass numbers A to facilitate comparison.

l_h/fm	r_n/fm	z_n/fm	A	$A_{cn} - A$
11.5	5.2	2.6	90	162
13.0	4.0	1.4	102	150
16.0	2.3	0.8	109	143
18.3	1.2	0.6	112	140
standard			$\bar{A}_L = 109$ [12]	
l_h/fm	r_n/fm	z_n/fm	A	$A_{cn} - A$
11.0	4.1	5.9	43	209
13.0	3.2	4.8	51	201
15.7	2.0	2.9	68	184
super-asymmetric			$\bar{A}_L \approx 65$ [12, 13]	

as in nature [4], and the largest attainable theoretical asymmetry for ^{236}U over that of ^{252}Cf is just the same as the measured ratio of asymmetries, similarly as pictured in Fig. 16 of [14].

b) Total Kinetic Energies

From data as in Fig. 3 one may extract three average total kinetic energies $\bar{E}_k$: 185.8 MeV is the total average over all partitions, but also the partial average over the standard component since it strongly prevails for ^{252}Cf (sf) [12, 13]. Crudely we can estimate that the deficit of the symmetrical component compared to 185.8 MeV is given by the depth of the dip, i. e. about 6 MeV. An approximate value for the average total kinetic energy of the super-asymmetrical component can also be taken directly from Fig. 3: 146 MeV.

Theoretically we get comparable energies as follows: We find from Fig. 1 $l_h = 14$, 15.7, 18.3, and 20.7 fm as scission lengths of the various channels. Using these lengths one may determine the potential energies $\bar{V}_{sciss}$ of repulsion between the nascent fragments by a procedure described in [15] and [16]. To be consistent, we had to rescale lengths because here in the Strutinsky calculations we used the Myers-Swiatecki [10] unit radius $r_0 = 1.2249$ fm for the liquid-drop part while it was $r_0 = 1.15$ fm in the calculations of [15, 16]. The thus obtained values are presented in Table 2. The agreement is as good as can be expected from the method. Just the repulsion energy $\bar{V}_{sciss}$ of the super-asymmetrical component is too high, but still it is in the correct order as being the smallest value of all.

Similar calculations for ^{236}U and ^{258}Fm indicate that, in the former case, the dip in $\bar{E}_k$(A) at symmetry should have the depth 22 MeV (experimentally 23 MeV [17]) and that, in the latter case, the super-short path is most probable; we find as potential energy of repulsion 236 MeV, to be compared with 232 MeV as measured total kinetic energy [4].

It is remarkable that the scission length calculated by a purely hydrodynamical model agrees with that of the standard channel. From [16] we find $l_h =$ 18.9 fm if scaling is done as just described, and we find $\bar{V}_{sciss} = 186$ MeV instead of 190 MeV as given in Table 2. This agreement takes place for all actinides, even for the heaviest ones.

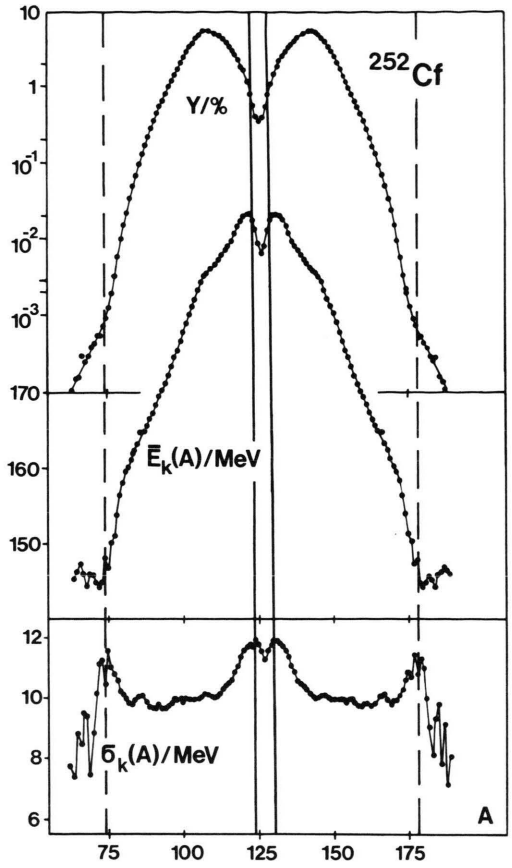

Fig. 3. From top to bottom: measured yield Y, average total kinetic energy $\bar{E}_k(A)$, and standard deviation $\sigma_k(A)$ of kinetic energy as functions of the mass number A of one of the fragments in the spontaneous fission of ^{252}Cf. The data are taken from [13]. The four parallel straight lines are to mark those values of A for which $\sigma_k(A)$ becomes maximum. These lines separate three components: The products of the super-long path can be seen preferentially between the solid lines. Between the solid and dashed lines there is the domain of the standard channel. The super-asymmetrical channel generates the wings beyond the dashed lines. Of course, fluctuations produce sizeable overlap between the components.

Table 2. Comparison between average kinetic energy $\bar{E}_k$ and average potential energy $\bar{V}_{sciss}$ of repulsion between the nascent fragments of ^{252}Cf. The first two columns contain experimental data concerning the average mass number $\bar{A}_L$ of the light fragment and $\bar{E}_k$ (cf. Sects. 2b and 2c). The next two columns reproduce the theoretical results from the present work.

$\bar{A}_L$	$\bar{E}_k$/MeV	$\bar{V}_{sciss}$/MeV	l_h/fm	Name
≈ 126	215–225?	229	14.0	super-short
65	146	164	15.7	super-asymmetric
109	185.8	190	18.3	standard
126	180	176	20.7	super-long

c) Neutron Multiplicities

Extremely long and certain short fission paths should both show up by enhanced neutron emission. The former because it produces fragments with strong prolate deformations, the latter because of pear-shaped deformations. All deformations should be transformed to heat, and heat finally causes neutron emission [15]. Peaks in the neutron multiplicity for nearly symmetrical fission of ^{252}Cf have been observed by Zakharova and Ryazanov at low and high total kinetic energies (Fig. 1 in [18]). More recent measurements by Budtz-Jørgensen et al. show that the data of [18], in particular at low kinetic energies cannot be completely correct [19]. But even the new measurements do not exclude enhanced neutron emission at very high and very low energies.

From these neutron multiplicities the entries with question mark in Table 2 were obtained. [18] suggests 225 MeV, [19] 215 MeV as total kinetic energy of the super-short component. However, more accurate data have still to be expected.

d) Relative Abundances

The graph of the potential energy $E_{gs} - E_{def}$ in Fig. 1 shows that the standard path has to overcome the lowest barrier, the super-short path a higher one, the super-long path a still higher one, and the super-asymmetrical path the highest one. Apart from the difficulty to detect the super-short channel, the same order occurs in the measured mass yields shown in Figure 3: The standard component is the most abundant, the super-long one at symmetry comes next, and the super-asymmetrical events are so rare that they were discovered only in the previous year.

The super-short path takes, as seen in Fig. 1, a long part of its course through asymmetry. It is therefore possible that it leads preferentially to slightly asymmetrical fission. It would then be buried under the wings of the standard component even if the super-short channel was not the rarest to be visited. New measurements indeed show that there is an "island" of very fast fragments close to symmetry [19]. These fragments are produced without excitation energy and should thus have still somewhat higher kinetic energies than those discussed in the previous paragraph. This is possible because all channels, in particular the super-short path, admit fluctuations.

These considerations are again corroborated by our results on the fission of ^{236}U and ^{258}Fm. In ^{236}U the super-short channel is not connected with the ground state, and the standard channel has, as in ^{252}Cf, a lower barrier than the super-long path. In ^{258}Fm the super-long path dissolves at $l_h = 17$ fm. The super-short path bifurcates from the standard path at a convenient place [5]. In ^{258}Fm the potential energy favors the super-short channel so that it becomes the most probable path, as observed experimentally [4].

4. Summary

The existence of the standard, the super-long, and the super-asymmetrical channels is confirmed by data on mass yield and total kinetic energy. Neutron multiplicity presently gives only for the standard channel unique evidence, namely by the famous sawtooth curve [16]. Nevertheless, neutron multiplicities and total kinetic energies already give indications for the super-short path too. New experiments or a better evaluation of existing data to

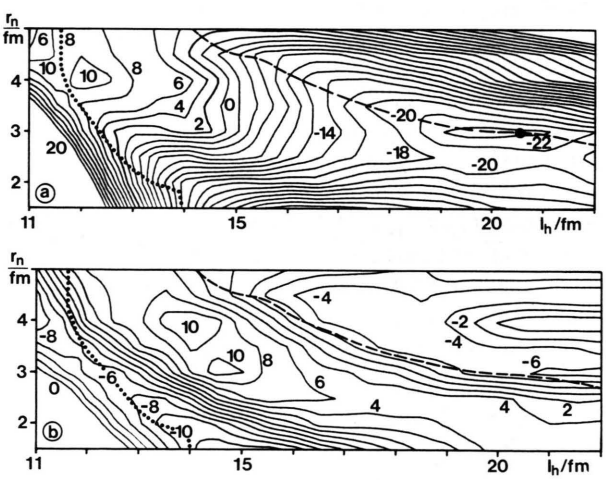

Fig. 4. Potential energy (part **a**) and shell corrections (part **b**) displayed as contour plots for ^{252}Cf in the (l_h, r_n) plane for symmetrical shapes ($z_n = 0$). The numbers at the lines give energies in MeV where negative values mean gain of energy. The super-short and super-long channels are easily recognized. Dots and dashes are taken from Figure 1. The standard and super-asymmetric channels cannot be seen because of their asymmetry. The fourth minimum is indicated in part **a** as a heavy dot. This is suspected to be the termination of the super-long channel (cf. Figure 1).

settle this problem are needed. Moreover, a complete deconvolution of existing data in terms of gaussians would be helpful because it would set much better standards for the comparison of experimental results with better calculations.

Our – theoretical – shortcomings at present are: The barriers we calculate are higher than the experimental ones [20]. As a consequence, we did not try a quantitative prediction of relative abundances. The deficiency comes from the liquid-drop model [10] with its parameters not optimized for the present purpose. Even more serious is the omission of dynamics. Fig. 4b gives an answer to both objections: The shell corrections in the super-short and the super-long paths are so strong that a better liquid-drop model and the inclusion of dynamics may modify but not abolish these channels. The same statement holds for the super-asymmetrical path.

One may ask if these channels were really due to shell effects since it was found that also the liquid drop energy alone yields several fission paths [21, 22]. These, however, are different from those discussed here: First, the unusual liquid-drop paths lead to multiple fragmentation. Second, Fig. 4 shows directly the shell corrections as the origin of the super-short and the super-long channels. It is seen that the effect is pleasantly large so that the Strutinsky method does not seem to be overtaxed. The standard path, on the other hand, closely corresponds to the usual liquid-drop fission path. Shell effects produce here just the asymmetry, but the length of the path remains nearly the same.

What is new in the preceding discussion? That the vicinity of the second saddle should be considered as the birth-place of mass asymmetry, was shown long ago [23, 7]. Pashkevich predicted two channels for lead [24]. We discovered now four channels. In the lighter actinides up to californium the standard and the super-long channels prevail; in the very heavy actinides fission proceeds through the super-short and the standard channels. The super-asymmetric channel is present in the heavier actinides including californium. In the lighter actinides it is replaced by a less asymmetric path which may be regarded as a splitting of the standard path. This survey seems to be unprecedented.

Discussions with J. Theobald and suggestions on this paper by him and H. J. Krappe were helpful. C. Budtz-Jørgensen and H.-H. Knitter gave us much new insight into the spontaneous fission of californium. We want to thank the GSI for financial support.

[1] A. Turkevich and J. B. Niday, Phys. Rev. **84,** 52 (1951).
[2] H. C. Britt, H. E. Wegner, and J. C. Gursky, Phys. Rev. **129,** 2239 (1963).
[3] M. G. Itkis, V. N. Okolovich, A. Ya. Rusanov, and G. N. Smirenkin, Z. Phys. **A320,** 433 (1985).
[4] E. K. Hulet, J. F. Wild, R. J. Dougan, R. W. Lougheed, J. H. Landrum, A. D. Dougan, M. Schädel, R. L. Hahn, P. A. Baisden, C. M. Henderson, R. J. Dupzyk, K. Sümmerer, and G. R. Bethune, Phys. Rev. Lett. **56,** 313 (1986).
[5] U. Brosa, S. Grossmann, and A. Müller, Z. Phys. A **325,** 241 (1986).
[6] V. M. Strutinsky, Nucl. Phys. **A95,** 420 (1967).
[7] H. C. Pauli, T. Ledergerber, and M. Brack, Phys. Lett. **34B,** 264 (1971).
[8] J. Dudek, W. Nazarewicz, and A. Faessler, Nucl. Phys. **A412,** 61 (1984) and the references therein.
[9] A. Sobiczewski, T. Krogulski, J. Blocki, and Z. Szymański, Nucl. Phys. **A168,** 519 (1971), variant (iii) of parameters.
[10] W. D. Myers and W. J. Swiatecki, Ark. Fys. **36,** 343 (1967).
[11] L. Wilets, Theories of Nuclear Fission, Clarendon Press, Oxford 1964, p. 46.
[12] G. Barreau, A. Sicre, F. Caitucoli, M. Ashgar, T. P. Doan, B. Leroux, G. Martinez, and T. Benfoughal, Nucl. Phys. **A432,** 411 (1985).
[13] C. Budtz-Jørgensen and H.-H. Knitter, in Proceedings of the Fifteenth International Symposium on Nuclear Physics, Gaussig 1985.
[14] P. Möller and J. R. Nix, in Proceedings of the Third International Atomic-Energy Agency Symposium on Physics and Chemistry of Fission, Rochester 1973 (IAEA, Vienna 1974), Vol. I, p. 103.
[15] U. Brosa and S. Grossmann, Z. Phys. **A310,** 177 (1983).
[16] U. Brosa, Phys. Rev. **C32,** 1438 (1985) and references therein.
[17] C. A. Straede, Neutron Induced Fission of ^{235}U (Thesis, CBNM Geel, 1985) and Ch. Straede, C. Budtz-Jørgensen, and H.-H. Knitter, to be published in Nucl. Phys. A.
[18] V. P. Zakharova and D. K. Ryazanov, Sov. J. Nucl. Phys. **30,** 19 (1979).
[19] C. Budtz-Jørgensen and H.-H. Knitter, Proc. Journée d'études sur la fission, Arachon 1986 and Proc. Seminar on Fission, Habay-La-Neuve (SCK; Mol 1986), p. 91.
[20] M. Dahlinger, D. Vermeulen, and K.-H. Schmidt, Nucl. Phys. **A376,** 94 (1982).
[21] W. J. Swiatecki, in Proceedings of the Second International Conference on the Peaceful Uses of Atomic Energy, Geneva 1958 (United Nations, New York 1958), Vol. XV, p. 248.
[22] V. M. Strutinsky, Sov. Physics JETP **15,** 1091 (1962).
[23] P. Möller and S. G. Nilsson, Phys. Lett. **31B,** 283 (1970).
[24] V. V. Pashkevich, Nucl. Phys. **A169,** 275 (1971).